Bioelectrochemistry 84 (2012) 32–37

Contents lists available at SciVerse ScienceDirect

Bioelectrochemistry

journal homepage: www.elsevier.com/locate/bioelechem

Gold nanoparticle-assembled capsules and their application as hydrogen peroxide biosensor based on hemoglobin

Jie Xuan [a], Xiang-dong Jia [a], Li-Ping Jiang [a,*], E.S. Abdel-Halim [b], Jun-Jie Zhu [a]

[a] State Key Lab of Analytical Chemistry for Life Science, School of Chemistry and Chemical Engineering, Nanjing University, Nanjing 210093, PR China
[b] Petrochemical Research Chair, Chemistry Department, College of Science, King Saud University, Riyadh 11451, P.O. Box 2455, Saudi Arabia

ARTICLE INFO

Article history:
Received 25 February 2011
Received in revised form 14 September 2011
Accepted 27 October 2011
Available online 4 November 2011

Keywords:
Gold nanoparticle-assembled capsules
Electrochemical biosensor
Hemoglobin

ABSTRACT

Gold nanoparticle-assembled capsules (GNACs) with controllable size and tunable morphology were fabricated through a simple two-step mixing procedure. Cationic polyelectrolyte was first induced to self-assemble into spherical aggregates in the presence of multivalent anions. Then, the aggregates served as an effective template for the self-assembly of gold nanoparticles to form size-controllable capsules. By adjusting the quantity of gold nanoparticles, capsules with various morphologies could be obtained. Because of their unique nanoporous features, the capsules with intact shells were further used to load hemoglobin (Hb) for the fabrication of a novel H_2O_2 biosensor. The results of UV–vis spectroscopy and cyclic voltammetry indicated that the capsules provided a suitable matrix for the immobilization of Hb. Additionally, the resulting biosensor showed a high affinity and good catalytic activity to H_2O_2. With the advantages of the large surface area, good conductivity and biocompatibility, the GNACs can offer a promising platform for the development of biosensors. Moreover, on the basis of the capsule structure, this material may also be expected to apply in some fields such as drug delivery, medical diagnostics and bio-encapsulation.

1. Introduction

In the past few decades, nanoparticles attracted considerable interest due to their unique photonic, electronic, magnetic, and catalytic properties. Numerous efforts have been devoted to the synthesis of various nanoparticles. With the tremendous success in precise control over the size and shape of nanoparticles, more attention has been paid to exploiting highly structured nanoparticle assemblies [1–4], which exhibit unique structure-dependent physical properties and are very promising for the construction of novel functional devices [5]. Especially, well-designed gold nanoparticle assemblies have emerged as exciting materials for optical, electronic, catalytic, and sensing applications [6]. To date, a number of strategies have been developed to organize gold nanoparticles into well-defined structure [6–11].

Since a variety of interactions such as hydrogen bonding, biospecific recognition, coordination, electrostatic, hydrophobic and dipole–dipole interactions can be employed in the process [12], self-assembly presents a particularly powerful tool for the preparation of structurally well-defined nanoparticle-based materials [13]. Recently, Wong et al. developed a facile and versatile route termed 'tandem self-assembly' or 'polymer aggregate templating' [14]. In their design, negatively charged nanoparticles effectively self-assemble into closed-shell structure through a simple two-step mixing procedure. Two kinds of hierarchically ordered microcapsules composed of silica (SiO_2) [15] and tin oxide (SnO_2) nanoparticles [16] were prepared with this method. For further application, the SiO_2 nanoparticle-assembled capsules acting as a new type of delivery vehicle were used for the encapsulation and release of the indocyanine green (ICG) [17]. However, some drawbacks such as poor electro-conductivity and low catalytic activity may limit their further applications.

Herein, we developed the 'tandem self-assembly' strategy to fabricate the gold nanoparticle-assembled capsules (GNACs). By adjusting the synthetic conditions, controllable size and tunable morphology were achieved. The scanning electron microscopy (SEM) results revealed that the intact gold shell possessed a unique nanoporous structure, which offered a promising matrix for biomolecular loading. By using hemoglobin (Hb) as a model, the Hb-GNACs 3D architecture was constructed. Once the bioconjugates were incorporated into a biosensor, a fast and effective direct electron transfer between the heme center of Hb and electrode was realized. The resulting biosensor showed good catalytic performance to hydrogen peroxide (H_2O_2) with a linear range of 1–140 μM and a detection limit of 0.93 μM at a signal-to-noise ratio (S/N) of 3. In addition, the small apparent Michaelis–Menten constant (K_M^{app}) indicated a high biological affinity of the immobilized Hb to H_2O_2.

2. Experimental

2.1. Chemicals

Poly (allylamine hydrochloride) (PAH) ($M_w \approx 15{,}000$) was purchased from Aldrich Chemical Co. H_2O_2 (30% w/v solution) of

* Corresponding author.
E-mail address: jianglp@nju.edu.cn (L.-P. Jiang).

1567-5394/$ – see front matter © 2011 Elsevier B.V. All rights reserved.
doi:10.1016/j.bioelechem.2011.10.007

analytical grade was obtained from Shanghai Biochemical Reagent Company (China). Nafion (5% w/w solution) was purchased from Alfa Aesar. Hb was purchased from Sigma and was used without further purification. All other reagents were of analytical grade. Ultrapure fresh water obtained from a Millipore water purification system (MilliQ, specific resistivity > 18 MΩ cm, S. A. Molsheim, France) was used throughout this work.

2.2. Apparatus

The morphology of the GNACs was characterized by transmission electron microscopy (TEM, JEOL JEM 2100) and field-emission scanning electron microscopy (FESEM, HITACHI S4800). UV–vis spectra were recorded on a Shimadzu UV-3600 spectrophotometer. Cyclic voltammetry (CV) measurements were performed on a CHI660B electrochemical workstation (Shanghai Chenhua, Shanghai, China). A conventional three-electrode system with the modified glassy carbon electrode (GCE) as the working electrode, a platinum wire as the auxiliary electrode, and a saturated calomel electrode (SCE) as the reference electrode was used in all electrochemical experiments. All electrolyte solutions were deoxygenated by bubbling highly pure nitrogen prior to experiments, and a nitrogen atmosphere was kept over the solutions during measurements.

2.3. Preparation of GNACs

Gold nanoparticles were prepared according to the literature [18] by using $NaBH_4$ as reductant and stabilized with sodium citrate, with the concentration of about 5.45×10^{-4} M (M = mol/L). GNACs were prepared through a simple two-step mixing procedure. In brief, 0.5 mL of Na_2HPO_4 solution with special concentration (0.01 M, 0.015 M or 0.02 M) was added to equal volume of 0.5 mg/mL PAH solution. After that, the mixture turned turbid, indicating the formation of polyelectrolyte-aggregates. The resulting suspension was shaken for 10 s and left to age for 30 min. Then, it was added to the colloidal gold solution and mixed for 40 min. After centrifugation and washing, the GNACs were finally obtained.

2.4. Preparation of Hb-GNACs bioconjugates

For the combination of Hb, the as-prepared GNACs were dispersed in 2 mL of 0.01 M phosphate buffer solution (PBS, pH = 6.0) containing 4 mg of Hb and shaken at room temperature for 12 h, followed by centrifugation and washing. The obtained bioconjugates were resuspended in 1 mL of 0.01 M PBS (pH = 7.0) and stored at 4 °C for further use.

2.5. Fabrication of the biosensor

A GCE with diameter of 3 mm was polished with 1.0, 0.3, and 0.05 μm alumina powder successively, followed by successive sonication in acetone and water. Then, 5 μL of the bioconjugates suspension prepared above was dropped on the surface of the pretreated GCE and left to dry in a silica gel desiccator. Finally, 2 μL of 0.5% Nafion aqueous solution was deposited to form a membrane. The resulting electrode was stored at 4 °C when not in use.

3. Results and discussion

3.1. Characterization of GNACs and Hb-GNACs

GNACs were fabricated through a simple two-step mixing procedure involving the admixture of cationic polymers (PAH) and multivalent anions (Na_2HPO_4) and the subsequently combination with negatively charged gold nanoparticles. The capsule structure can be directly observed in the transmission electron microscopy (TEM) image (Fig. 1).

The formation mechanism is illustrated in Scheme 1. In the first step, multivalent anions acted as ionic cross-linkers leading to the formation of globular polyelectrolyte-aggregates with positively charged surfaces [17]; then negatively charged gold nanoparticles assembled around the polyelectrolyte-aggregates by the electrostatic attractions so that the GNACs were obtained. In brief, the synthetic route can be described as a self-assembly process with multivalent anions induced polyelectrolyte-aggregates as template. Therefore, the resulting capsules are sensitive to the conditions for the aggregation of polyelectrolyte.

Fig. 2 shows the scanning electron microscopy (SEM) images of the GNACs obtained at different *R*, which is defined as the ratio of total negative charges from the multivalent anion to the total positive charges from the cationic polyelectrolyte. The resulting capsules were uniform in size and morphology at each *R* value, while the average diameter of the capsules increased with *R* rising, which was 300 nm at $R=4$, 700 nm at $R=6$, and 1200 nm at $R=8$, respectively. This indicated that size-controllable GNACs could be prepared by varying the value of *R*. Herein, the GNACs with small size (prepared at $R=4$) were chosen for the further study due to their high specific surface area.

To investigate the self-assembly behavior of gold nanoparticles, various quantities of the colloidal gold solutions were introduced, and the capsules with tunable morphologies were obtained accordingly. In order to get a clear observation, the capsules with large size ($R=8$) were chosen as models. As shown in Fig. 3(a), numerous gold floccules spread around the globular polyelectrolyte-aggregates template when the polyelectrolyte-aggregates suspension was mixed with twice volume of the colloidal gold solution. With the quantity of the colloidal gold increasing to 4 times that of the polyelectrolyte-aggregates suspension, many hill-like gold nanoparticle-assemblages formed on the template surface, as can be seen in Fig. 3(b). Further increase in the quantity of the colloidal gold led to a rough gold shell with several cracks surrounding the polyelectrolyte-aggregates template, as shown in Fig. 3(c). When the quantity of the colloidal gold was up to 10 times, capsules with intact shells were obtained as shown in Fig. 3(d), and it was worth noting that the supernatant liquor after centrifugation was no longer colorless but kept the color of the colloidal gold solution. This phenomenon indicated that the self-assembly of gold nanoparticles reached saturation. Although all the cracks were filled up, it was obvious that the intact gold shell still possessed a nanoporous feature, which offered a promising interface with good conductivity and considerably large surface area. Thus, the capsules with intact shells were expected to be an effective candidate for biomolecular immobilization and biosensor fabrication. By using Hb as a model, the Hb-GNACs composite was prepared to construct a novel H_2O_2 biosensor. As can be observed in Fig. 4, the surface texture of the composite became indistinct after the immobilization of Hb.

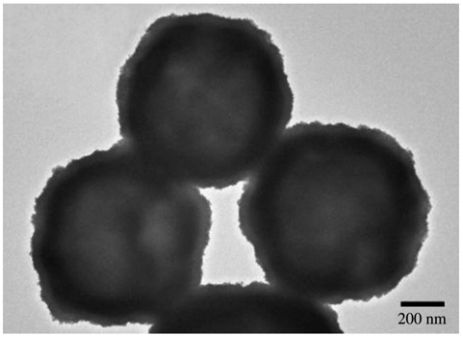

Fig. 1. TEM image of GNACs.

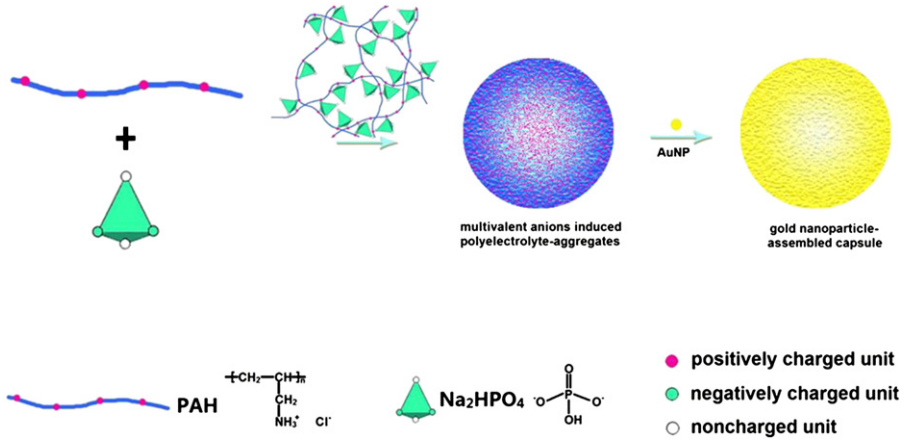

Scheme 1. Formation process of the gold nanoparticle-assembled capsule.

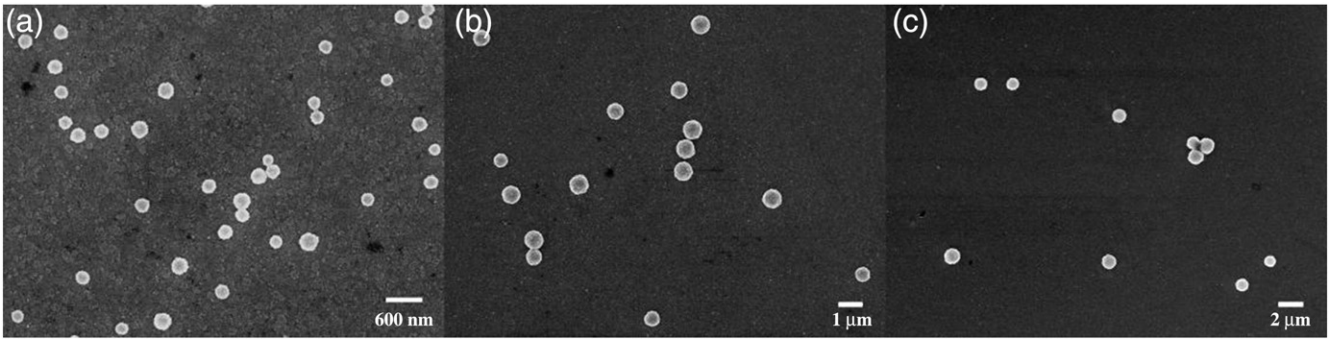

Fig. 2. SEM images of GNACs obtained at different *R*: (a) $R=4$; (b) $R=6$; (c) $R=8$.

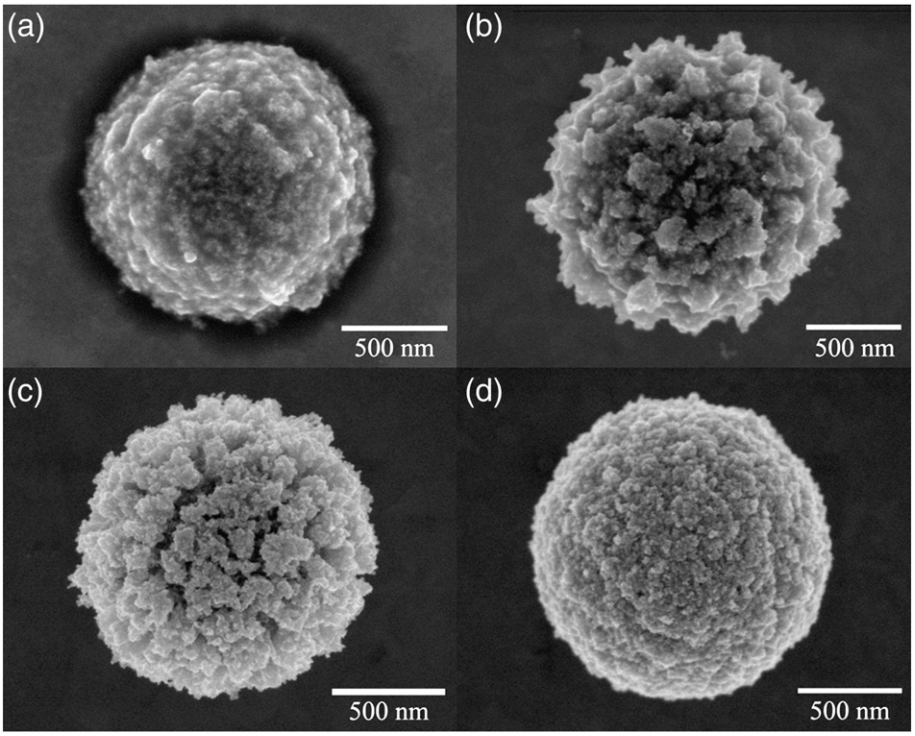

Fig. 3. Typical SEM images of GNACs prepared at $R=8$ with different quantities of the colloidal gold solution: (a) twice the volume of the polyelectrolyte-aggregates suspension; (b) 4 times the volume of the polyelectrolyte-aggregates suspension; (c) 8 times the volume of the polyelectrolyte-aggregates suspension; (d) 10 times the volume of the polyelectrolyte-aggregates suspension.

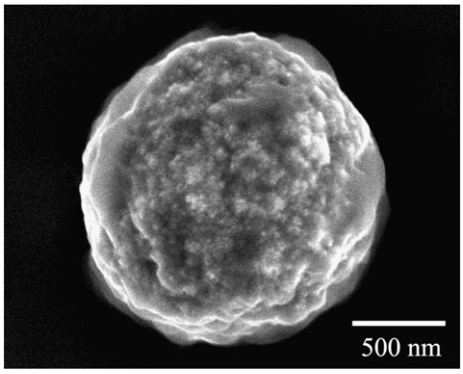

Fig. 4. SEM image of the Hb-GNACs composite prepared at R = 8.

UV–vis spectroscopy was used to monitor the modification process. As shown in Fig. 5, the as-prepared GNACs exhibited a wide absorption band from 500 nm to 750 nm (curve c), while the characteristic surface plasmon resonance band of colloidal gold appeared at 512 nm (curve b). This red shift as well as the broadening of the band could be attributed to the formation of gold nanoparticle assemblies, which led to a collective surface plasmon oscillation [10]. After the loading of Hb, a characteristic Soret band of prosthetic heme group appeared at 408 nm (curve a), while that of native Hb was located at 406 nm (curve d). This slight red shift of 2 nm indicated the interaction between Hb and GNACs. What's more, such a small difference also suggested that the immobilized Hb was not grossly denatured and the GNACs provided a suitable microenvironment for Hb to retain its native structure.

3.2. Direct electrochemistry of Hb-GNACs/Nafion modified electrode

The electrochemical behavior of the immobilized Hb was studied. Fig. 6 shows typical cyclic voltammograms (CVs) of different modified GCEs in 0.1 M PBS (pH = 7.0) at 100 mV s^{-1}. No obvious redox peaks were observed at the GNACs/Nafion modified GCE (curve c), indicating electro-inactivity of the material in the potential range. A couple of unconspicuous redox peaks were observed at the Hb/Nafion modified GCE (curve b), which could be ascribed to the direct electron transfer between Hb and the electrode. In contrast, a pair of stable and well-defined redox peaks could be observed at the Hb-GNACs/Nafion modified GCE (curve a), which indicated that the GNACs not only provided a favorable microenvironment for the

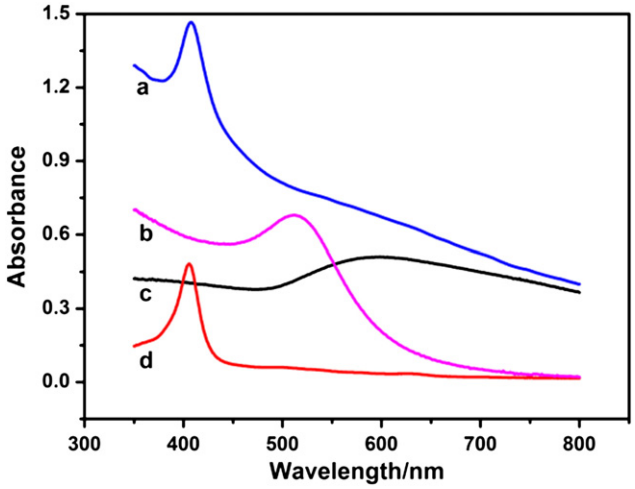

Fig. 5. UV–vis spectra of (a) Hb-GNACs, (b) gold nanoparticles, (c) GNACs, and (d) Hb solution.

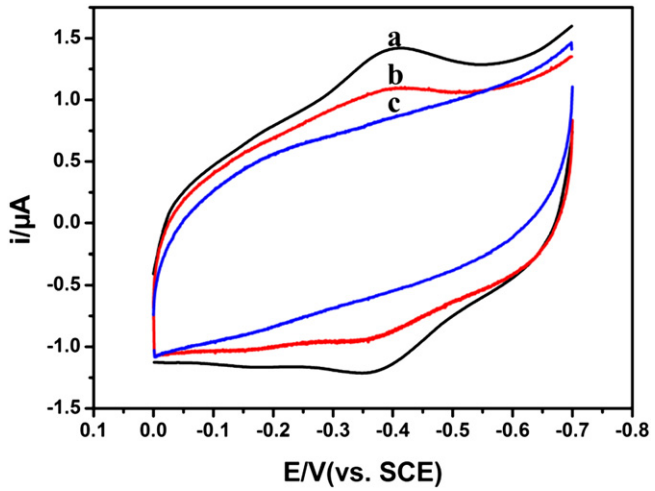

Fig. 6. CVs of (a) Hb-GNACs/Nafion, (b) Hb/Nafion, and (c) GNACs/Nafion modified GCEs in 0.1 M PBS (pH = 7.0) at 100 mV s^{-1}.

immobilized Hb molecules to retain their activity, but also greatly facilitated the direct electron transfer between the immobilized Hb and the electrode. The cathodic and anodic peak potentials observed at the Hb-GNACs/Nafion modified GCE were located at −0.405 V (vs. SCE) and −0.357 V (vs. SCE) respectively. This small peak-to-peak separation of 48 mV suggested a fast and quasi-reversible electron-transfer process [19]. When the peak-to-peak separation was less than 200/n mV, the apparent heterogeneous electron transfer rate constant (k_s) could be calculated according to the equation $k_s = mnFv/RT$ [20], where m is a parameter related to the peak-to-peak separation, n is the number of electrons, F is Faraday constant, v is the scan rate, R is ideal gas constant, and T is the temperature. For the Hb-GNAC/Nafion modified GCE, the value of k_s was estimated to be 2.64 s^{-1}, which was much larger than those reported previously [21–23]. This result further demonstrated that the GNACs acted as conducting channels helping to realize a faster and more effective direct electron transfer between the immobilized Hb and the electrode.

To study the electron transfer process further, the effect of scan rate on the electrochemical response of the immobilized Hb was also discussed. As shown in Fig. 7, both cathodic and anodic peak currents increased linearly with the scan rate rising from 50 mV s^{-1} to 600 mV s^{-1}. The linear regression equations were $i_p/\mu A = 0.00148v/(mV/s) - 0.02489$ for cathodic currents and $i_p/\mu A = -0.00137v/(mV/s) + 0.01952$ for anodic currents. This linearity with respect to v, and not to $v^{1/2}$, indicated a surface-controlled electrochemical process. According to Faraday's law, $Q = nFA\Gamma$, where Q can be obtained by integrating the reduction peak of Hb, F is Faraday constant, n and A stand for the number of electrons and the surface area of the electrode, respectively, the average surface concentration of electroactive Hb(Γ) at the Hb-GNACs/Nafion modified GCE was estimated to be 2.17×10^{-10} mol cm^{-2}, which was about 11 times that of the theoretical monolayer coverage of Hb ($\approx 1.89 \times 10^{-11}$ mol cm^{-2} [19]). Such a large quantity of electroactive Hb molecules participating in the electron-transfer process suggested that the GNACs offered a suitable matrix for Hb loading.

3.3. Electrocatalytic properties of the Hb-GNACs/Nafion modified electrode towards H_2O_2

The electrocatalytic activity of the immobilized Hb towards H_2O_2 was investigated by cyclic voltammetry, as shown in Fig. 8(a). With the successive addition of H_2O_2, the cathodic current of the Hb-GNACs/Nafion modified GCE gradually increased, while the corresponding anodic current decreased, indicating a typical

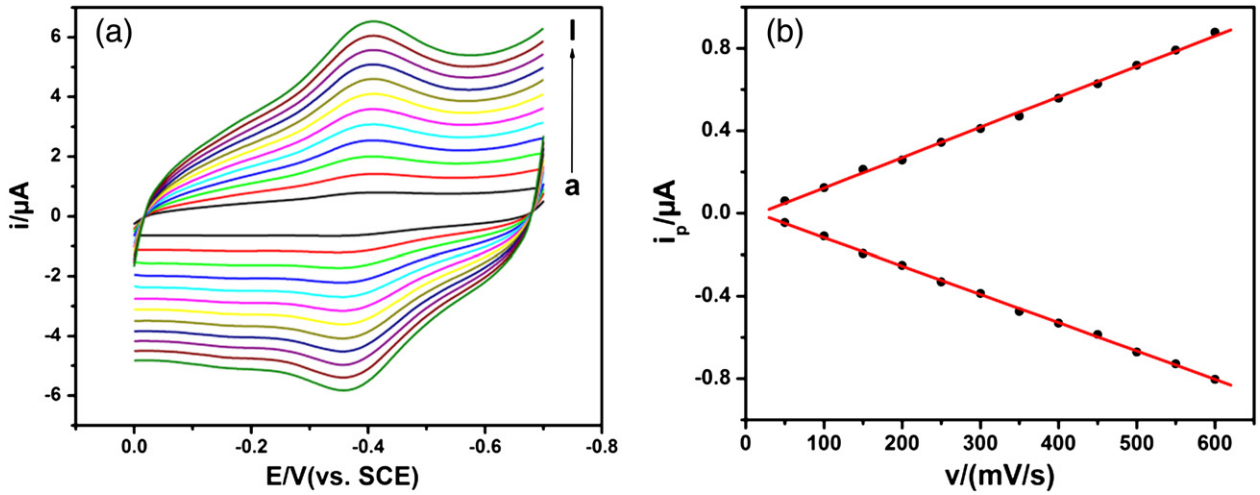

Fig. 7. (a) CVs of Hb-GNACs/Nafion modified GCE in 0.1 M PBS (pH = 7.0) at different scan rates (mV s^{-1}): (a) 50, (b) 100, (c) 150, (d) 200, (e) 250, (f) 300, (g) 350, (h)400, (i) 450, (j) 500, (k) 550, (l) 600. (b) Plots of anodic and cathodic peak currents vs. scan rates.

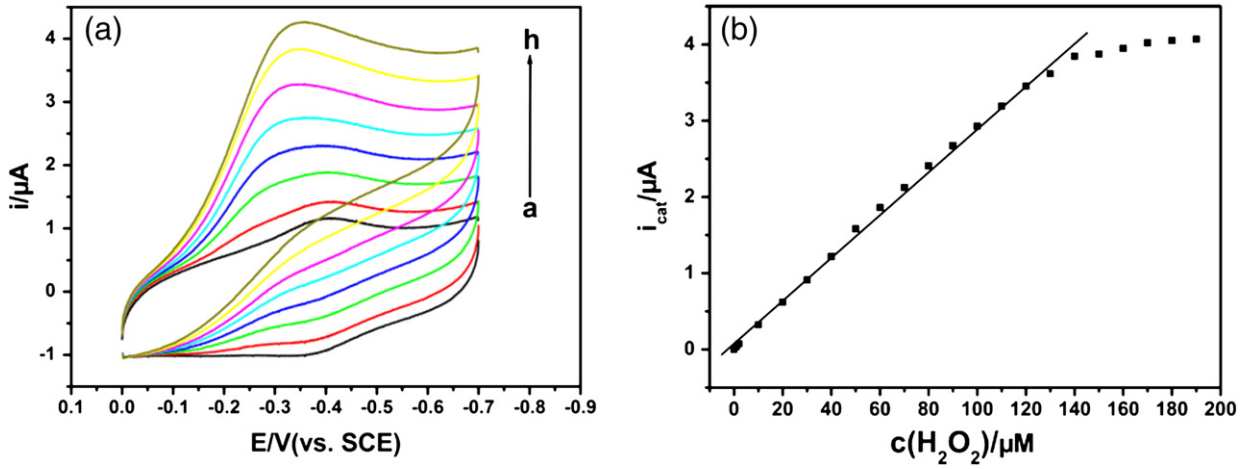

Fig. 8. (a) CVs of Hb-GNACs/Nafion modified GCE in 0.1 M PBS (pH = 7.0) containing: (a) 0, (b) 10, (c) 30, (d) 50, (e) 70, (f) 90, (g) 110, and (h)130 μM H_2O_2 at 100 mV s^{-1}. (b) Calibration curve of electrocatalytic current to H_2O_2 concentration.

electrocatalytic reduction process of H_2O_2. Since this phenomenon was not observed at the GNACs/Nafion modified GCE, it can be concluded that the catalytic reduction of H_2O_2 was attributed to the presence of Hb. A possible mechanism of the catalytic reaction might be expressed as follows [19,24]:

$$\mathrm{Hb[Heme(Fe^{III})] + H_2O_2 \rightarrow Compound\ I + H_2O} \quad (1)$$

$$\mathrm{Compound\ I + H_2O_2 \rightarrow Hb[Heme(FeIII)] + H_2O + O_2} \quad (2)$$

$$\mathrm{Hb[Heme(Fe^{III})] + H^+ + e^- \rightarrow Hb[Heme(Fe^{II})](at\ electrode)} \quad (3)$$

$$\mathrm{Hb[Heme(Fe^{II})] + O_2 \rightarrow Hb[Heme(Fe^{II})] - O_2\ fast} \quad (4)$$

$$\mathrm{Hb[Heme(Fe^{II})] - O_2 + H^+ + e^- \rightarrow Hb[Heme(Fe^{III})] + H_2O_2(at\ electrode)} \quad (5)$$

The overall reaction of (1)–(5) would be:

$$\mathrm{H_2O_2 + 2H^+ + 2e^- \rightarrow 2H_2O.} \quad (6)$$

With the addition of hydrogen peroxide, it diffuses to the surface of the electrode and oxidizes Hb[Heme(Fe^{III})] to compound I, which is quite instable and immediately reacts with H_2O_2 to return to Hb [Heme(Fe^{III})]. In this process, oxygen is formed. As the potential decreased negatively, Hb[Heme(Fe^{III})] is reduced to Hb[Heme(Fe^{II})], which reacts rapidly with the oxygen to give Hb[Heme(FeII)]-O_2 [24]. And then H_2O_2 is regenerated by the electrochemical reduction of Hb[Heme(FeII)]-O_2. Therefore, oxygen and the resulted Hb[Heme (Fe^{II})]-O_2 promotes the catalytic cycle and is extremely important to the catalytic current in this reaction. What's more, to ensure the linear relationship between the electrocatalytic current and the concentration of the H_2O_2, deoxygenation is necessary in this system.

Fig. 8(b) shows the calibration curve of the catalytic current to the concentration of H_2O_2. Here the catalytic current (i_{cat}) is defined as the difference between the cathodic peak currents in the presence and in the absence of H_2O_2. It can be observed that the catalytic current increased linearly with the concentration of H_2O_2 increasing from 1 to 140 μM. The linear regression equation was $i_{cat}/\mu A = 0.0281c(H_2O_2)/$

μM(M = mol/L) + 0.0752 with a correlation coefficient of 0.998, and the detection limit was estimated to be 0.93 μM at a signal-to-noise ratio (*S*/*N*) of 3. When the concentration of H_2O_2 was higher than 140 μM, a response plateau was observed, indicating a typical Michaelis–Menten kinetic characteristic. The apparent Michaelis–Menten constant (*K*app M) was determined to be 0.21 mM according to the electrochemical version of Lineweaver–Burk equation [25]. This value is much smaller than those of 2.87 mM for the Hb/Au-SBA-15 modified GCE [26], 1.4 mM for the Hb/Chit-Aus/Cys modified Au electrode [27] and 0.77 mM for the Hb-CdTe-$CaCO_3$@PEs modified GCE [28], suggesting a higher affinity of the immobilized Hb to H_2O_2.

As a H_2O_2 biosensor, the reproducibility and stability of the Hb-GNACs/Nafion modified GCE were investigated. The relative standard deviation (R.S.D.) of the responses to 50 μM H_2O_2 was 3.7% for six successive measurements, indicating an acceptable reproducibility. Stability of the biosensor was investigated by consecutive calibrations curves at a constant potential of −0.40 V and the result also demonstrated a good stability. When not in use, the electrode was stored at 4 °C. It retained 93.6% of its original response after one-month storage, demonstrating a good long-term stability.

4. Conclusions

A rapid two-step mixing procedure was employed to fabricate gold nanoparticle-assembled capsules (GNACs). The rough surface with a nanoporous feature of the capsule offered an ideal interface for Hb loading. The results of UV–vis spectroscopy and cyclic voltammetry indicated that the capsules not only provided a suitable microenvironment for Hb to retain its activity, but also acted as conducting channels facilitating the direct electron transfer between the heme center of Hb and the electrode. As a biosensor, the resulting electrode showed a high affinity and good catalytic activity to H_2O_2 with good reproducibility and stability. Hydrogen peroxide is not only an essential mediator in food, clinical, environmental and many other fields, but also a by-product of various enzymatic reactions. Therefore, the as-prepared sensor could be used in the detection of H_2O_2 in real samples like disinfector, commercial contact lens solution or environmental samples, and it could also be used in the detection of antigen or antibody in real serum samples based on the peroxidase labeled immunoassay. Although deoxygenation is needed, the prepared sensor still owes an acceptable sensitivity due to the mechanism of the catalytic reaction. It was believed that the prepared GNACs provided a promising platform for the development of novel biosensors. Moreover, as its unique capsule structure, the material may also be an effective candidate for wide potential applications in encapsulation, protection and drug delivery.

Acknowledgments

We greatly appreciate the support of the National Natural Science Foundation of China for General Program (21075061) and the Natural Science Foundation of Jiangsu Province of China (BK2010363). This work is also supported by the International S&T Cooperation Projects of China (2010DFA42060) and the Fundamental Research Funds for the Central Universities (1105020503 and 1116020507).

References

[1] M.S. Wong, J.N. Cha, K.S. Choi, T.J. Deming, G.D. Stucky, Assembly of nanoparticles into hollow spheres using block copolypeptides, Nano Lett. 2 (2002) 583–587.
[2] V.S. Murthy, J.N. Cha, G.D. Stucky, M.S. Wong, Charge-driven flocculation of poly (L-lysine)-gold nanoparticle assemblies leading to hollow microspheres, J. Am. Chem. Soc. 126 (2004) 5292–5299.
[3] P. Arumugam, H. Xu, S. Srivastava, V.M. Rotello, 'Bricks and mortar' nanoparticle self-assembly using polymers, Polym. Int. 56 (2007) 461–466.
[4] F. Caruso, Hollow capsule processing through colloidal templating and self-assembly, Chem. Eur. J. 6 (2000) 413–419.
[5] R. Shenhar, E. Jeoung, S. Srivastava, T.B. Norsten, V.M. Rotello, Crosslinked nanoparticle stripes and hexagonal networks obtained via selective patterning of block copolymer thin films, Adv. Mater. 17 (2005) 2206–2210.
[6] F.A. Aldaye, H.F. Sleiman, Dynamic DNA templates for discrete gold nanoparticle assemblies: control of geometry, modularity, write/erase and structural switching, J. Am. Chem. Soc. 129 (2007) 4130–4131.
[7] A.K. Boal, F. Ilhan, J.E. DeRouchey, T. Thurn-Albrecht, T.P. Russell, V.M. Rotello, Self-assembly of nanoparticles into structured spherical and network aggregates, Nature 404 (2000) 746–748.
[8] M. Kimura, S. Kobayashi, T. Kuroda, K. Hanabusa, H. Shirai, Assembly of gold nanoparticles into fibrous aggregates using thiol-terminated gelators, Adv. Mater. 16 (2004) 335–338.
[9] S.F. Pang, T. Kondo, T. Kawai, Formation of dendrimer-like gold nanoparticle assemblies, Chem. Mater. 17 (2005) 3636–3641.
[10] S.S. Kinge, M. Crego-Calama, D.N. Reinhoudt, Gold nanoparticle assemblies through hydrogen-bonded supramolecular mediators, Langmuir 23 (2007) 8772–8777.
[11] J. Han, Y. Liu, R. Guo, Reactive template method to synthesize gold nanoparticles with controllable size and morphology supported on shells of polymer hollow microspheres and their application for aerobic alcohol oxidation in water, Adv. Funct. Mater. 19 (2009) 1112–1117.
[12] Z.Y. Tang, N.A. Kotov, One-dimensional assemblies of nanoparticles: preparation, properties, and promise, Adv. Mater. 17 (2005) 951–962.
[13] Y.P. Wang, H.P. Xu, X. Zhang, Tuning the amphiphilicity of building blocks: controlled self-assembly and disassembly for functional supramolecular materials, Adv. Mater. 21 (2009) 2849–2864.
[14] V.S. Murthy, R.K. Rana, M.S. Wong, Nanoparticle-assembled capsule synthesis: formation of colloidal polyamine-salt intermediates, J. Phys. Chem. B 110 (2006) 25619–25627.
[15] R.K. Rana, V.S. Murthy, J. Yu, M.S. Wong, Nanoparticle self-assembly of hierarchically ordered microcapsule structures, Adv. Mater. 17 (2005) 1145–1150.
[16] J. Yu, V.S. Murthy, R.K. Rana, M.S. Wong, Synthesis of nanoparticle-assembled tin oxide/polymer microcapsules, Chem. Commun. 10 (2006) 1097–1099.
[17] J. Yu, M.A. Yaseen, B. Anvari, M.S. Wong, Synthesis of near-infrared-absorbing nanoparticle-assembled capsules, Chem. Mater. 19 (2007) 1277–1284.
[18] B.D. Busbee, S.O. Obare, C.J. Murphy, An improved synthesis of high-aspect-ratio gold nanorods, Adv. Mater. 15 (2003) 414–416.
[19] X.B. Lu, J.H. Zhou, W. Lu, Q. Liu, J.H. Li, Carbon nanofiber-based composites for the construction of mediator-free biosensors, Biosens. Bioelectron. 23 (2008) 1236–1243.
[20] E.J. Laviron, The use of linear potential sweep voltammetry and of A.C. voltammetry for the study of the surface electrochemical reaction of strongly adsorbed systems and of redox modified electrodes, Electroanal. Chem. 100 (1979) 263–270.
[21] H.Y. Gu, A.M. Yu, H.Y. Chen, Direct electron transfer and characterization of hemoglobin immobilized on a Au colloid–cysteamine-modified gold electrode, J. Electroanal. Chem. 516 (2001) 119–126.
[22] J.J. Zhang, Y.G. Liu, L.P. Jiang, J.J. Zhu, Synthesis, characterizations of silica-coated gold nanorods and its applications in electroanalysis of hemoglobin, Electrochem. Commun. 10 (2008) 355–358.
[23] Y.D. Zhao, Y.H. Bi, W.D. Zhang, Q.M. Luo, The interface behavior of hemoglobin at carbon nanotube and the detection for H_2O_2, Talanta 65 (2005) 489–494.
[24] A.C. Onuoha, X. Zu, J.F. Rusling, Electrochemical generation and reactions of ferrylmyoglobins in water and microemulsions, J. Am. Chem. Soc. 119 (1997) 3979–3986.
[25] R.A. Kamin, G.S. Wilson, Rotating ring-disk enzyme electrode for biocatalysis kinetic studies and characterization of the immobilized enzyme layer, Anal. Chem. 52 (1980) 1198–1205.
[26] Y.Z. Xian, Y. Xian, L.H. Zhou, F.H. Wu, Y. Ling, L.T. Jin, Encapsulation hemoglobin in ordered mesoporous silicas: influence factors for immobilization and bioelectrochemistry, Electrochem. Commun. 9 (2007) 142–148.
[27] J.J. Feng, G. Zhao, J.J. Xu, H.Y. Chen, Direct electrochemistry and electrocatalysis of heme proteins immobilized on gold nanoparticles stabilized by chitosan, Anal. Biochem. 342 (2005) 280–286.
[28] W.Y. Cai, L.D. Feng, S.H. Liu, J.J. Zhu, 3D architecture: fabrication, characterization, and application in biosensing, Adv. Funct. Mater. 18 (2008) 3127–3136.